SHORTENING THE WAY TO EXPERIMENTAL EVIDENCE FOR HIGH-RANK SYMMETRIES IN ATOMIC NUCLEI: RESEARCHER INSTRUCTIONS*

J. Dudek[a,b], I. Dedes[a], J. Yang[a], A. Baran[a], D. Curien[b]
S. Tagami[c], Y.R. Shimizu[c] H.L. Wang[b,d]

[a]Institute of Physics, Maria Curie-Skłodowska University
pl. Marii Curie-Skłodowskiej 1, 20-031 Lublin, Poland
[b]Université de Strasbourg, IPHC
23, rue du Loess, 67037 Strasbourg, France
and
CNRS, UMR7178, 67037 Strasbourg, France
[c]Department of Physics, Faculty of Sciences, Kyushu University
Fukuoka 8190359, Japan
[d]School of Physics and Engineering, Zhengzhou University
Zhengzhou 450001, China

(Received December 21, 2018)

We discuss criteria for experimental identification of the nuclear tetrahedral and octahedral so-called high-rank symmetries based on the mean-field and group representation theories. We examine the possibly largest search zones on the (Z, N)-plane: in addition to traditionally discussed areas of even–even nuclei with proton and neutron numbers surrounding the tetrahedral magic ones ($Z_0^{\rm t}, N_0^{\rm t}$ = 32, 40, 56, 64, 70, 90, 112, 136), we discuss also the odd–even and even–odd nuclei for which the identification criteria non-trivially differ from those for the even–even ones. We also propose the appropriately chosen particle–hole excited states to profit from the deformation driving mechanism contributed by combinations of certain orbitals. The discussion is summarised in the form of a series of 'user' instructions.

DOI:10.5506/APhysPolBSupp.12.569

1. Introduction

In this article, we give a short account of the methods of identification of tetrahedral and octahedral symmetry shapes in atomic nuclei with the help

* Presented at the XXV Nuclear Physics Workshop "Structure and Dynamics of Atomic Nuclei", Kazimierz Dolny, Poland, September 25–30, 2018.

of the nuclear mean-field theory and the point-group representation theories. We apply these concepts not only to the lowest-energy configurations in the even–even nuclei (most often addressed in the literature), but also to the odd-A nuclei, and certain excited configurations which involve tetrahedral-deformation driving orbitals.

Since due to the short range of the nuclear interactions the shape of the nucleonic distributions in nuclei follows that of the equipotential surfaces of the mean-field potential, it follows that the shape symmetries are closely related to those of the associated mean-field Hamiltonian.

It has been suggested over 20 years back, Ref. [1], that in some atomic nuclei, well-pronounced potential energy minima may exist corresponding to the tetrahedral symmetry shapes. The authors examined the nuclear stability effects due to the spinor (so-called double) tetrahedral ($\mathrm{T}_{\mathrm{d}}^{\mathrm{D}}$) point-group of symmetry of the mean-field Hamiltonian and pointed to the physical consequences of the presence of three irreducible representations of the group in question, two non-equivalent 2-dimensional ones, and one 4-dimensional one.

The presence of the three irreducible representations implies that the single-nucleon levels generated by the Hamiltonian with such a symmetry form three independent families, as opposed to the two families of positive and negative parity orbitals in the 'usual' case. The four-dimensional irreducible representation implies the presence of the four-fold degenerate levels. This four-fold degeneracy has never been observed so far but it has fascinating quantum consequences in addition to the presence *per se*, such as an existence of 16-fold degenerate particle–hole excited states in the nuclear spectra. Moreover, the existence of four-fold degeneracies implies a systematic increase of the average level spacing in the single-nucleon spectra and facilitates creating relatively big shell-gaps usually referred to as tetrahedral magic gaps, see Fig. 1.

It has been shown in Ref. [1] that the tetrahedral symmetry implies the presence of the new magic numbers at Z_0^{t}, $N_0^{\mathrm{t}} = 56$, 64, 70, 90, 100, 112, 136. It has also been indicated that the three irreducible representations, denoted E, E* and G, can easily be identified and used for the level-labelling, an interesting alternative to the Nilsson labelling in this case, *cf.* Figs. 3 and 4 of Ref. [1].

The first case of experimental evidence for the tetrahedral symmetry, in ^{152}Sm, has been announced in Ref. [2]. The mean-field single-nucleon spectra for this nucleus are illustrated in Fig. 1 showing the tetrahedral shell gaps and low-level density areas opening when deformation increases.

The extension of the above considerations predicting the presence of the tetrahedral symmetry islands all over the (Z, N)-plane has been presented in Ref. [3], whereas a possible coexistence between the tetrahedral and octahedral symmetries has been presented in Ref. [5] focussing on the rare-earth

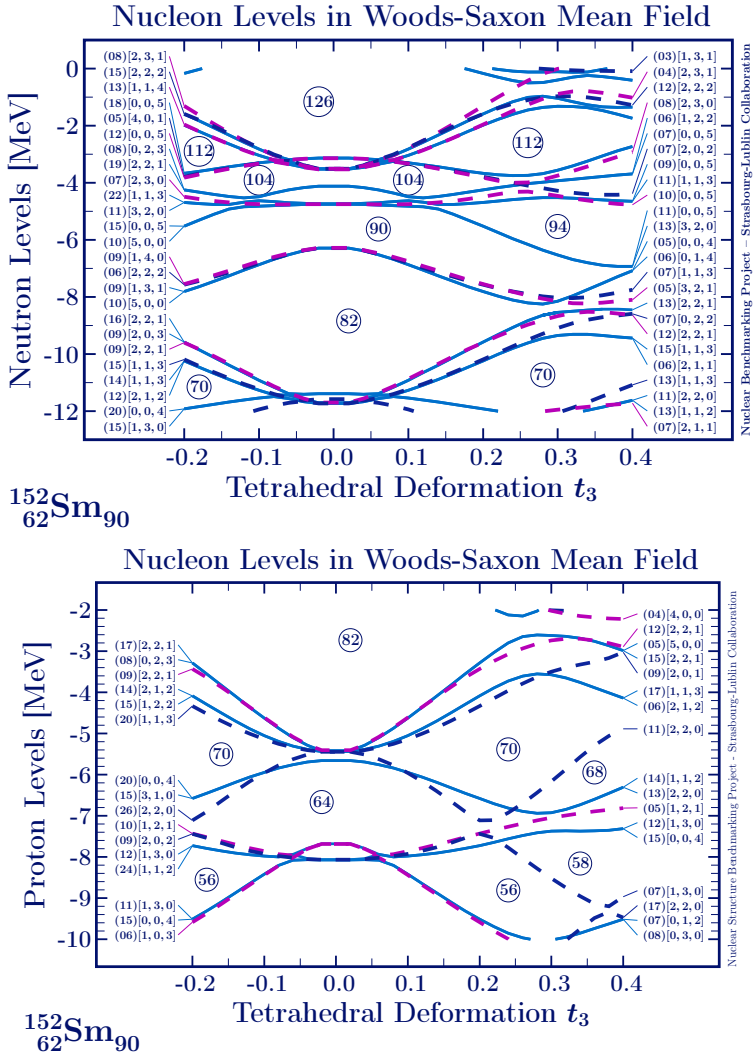

Fig. 1. Single-nucleon levels as functions of tetrahedral deformation, $t_3 \equiv \alpha_{32}$, calculated using the Woods–Saxon Universal phenomenological mean field, Ref. [4]. Top — neutrons, bottom — protons. We use Cartesian labels, coefficients in round parentheses give the probability amplitude related to each given label.

nuclei. The latter coexistence is of particular interest from the group theory point of view given the fact that the tetrahedral group is a subgroup of the octahedral one, $\mathrm{T_d} \subset \mathrm{O_h}$.

2. The link between the microscopic mean-field with high-rank symmetries and collective rotation

In the more recent articles, Refs. [6–8], the authors employed the newly written numerical code solving the Hartree–Fock–Bogolyubov problem with the Gogny interaction Hamiltonian allowing to break all geometrical symmetries. The algorithm employed the angular momentum and particle number projection techniques. Below, we focus on the mean field and the collective rotor properties separately.

2.1. The mean field within Hartree–Fock–Bogolyubov approach

The standard two-body Hamiltonian written down in a certain one-body basis whose states are enumerated with $\ell_i = 1, 2, \ldots M$, and $i = 1, 2, 3, 4$, has the usual form of

$$\hat{H} = \sum_{\ell_1 \ell_2} t_{\ell_1 \ell_2} \hat{c}^+_{\ell_1} \hat{c}_{\ell_2} + \tfrac{1}{2} \sum_{\ell_1 \ell_2} \sum_{\ell_3 \ell_4} v_{\ell_1 \ell_2 \ell_3 \ell_4} \hat{c}^+_{\ell_1} \hat{c}^+_{\ell_2} \hat{c}_{\ell_4} \hat{c}_{\ell_3} \,. \tag{1}$$

With the help of the Bogolyubov transformation leading from the particle state representation, $\{\hat{c}^+, \hat{c}\}$, to the quasi-particle representation, $\{\hat{\beta}^+, \hat{\beta}\}$,

$$\hat{\beta}^+_k \equiv \sum_{\ell} \left[U_{\ell k} \hat{c}^+_{\ell} + V_{\ell k} \hat{c}_{\ell} \right] \,, \tag{2}$$

with $\hat{\beta}$ denoting a Hermitian conjugate of the former, whereas the quasiparticle vacuum $|\Phi\rangle$ can be expressed using Thouless theorem

$$\begin{aligned} |\Phi\rangle \;&=\; \mathcal{N}\, e^{\hat{Z}} |0\rangle \,, \qquad \hat{Z} \equiv \tfrac{1}{2} \sum_{\ell' \ell} Z_{\ell' \ell} \hat{c}^+_{\ell'} \hat{c}^+_{\ell} \,, \\ \mathcal{N} \;&\equiv\; \langle 0 | \Phi \rangle \,, \qquad Z_{\ell' \ell} = \left(V U^{-1} \right)^*_{\ell' \ell} \,. \end{aligned} \tag{3}$$

After obtaining the constrained HFB state $|\Phi\rangle$, the quantum number projection is performed to obtain the projected wave functions of both parities

$$\left| \Psi^{INZ(\pm)}_{M;\alpha} \right\rangle = \sum_{K} g^{INZ(\pm)}_{K,\alpha} \, \hat{P}^I_{MK} \hat{P}_{\pm} \hat{P}^N \hat{P}^Z |\Phi\rangle \,, \tag{4}$$

where the amplitudes $g^{INZ(\pm)}_{K,\alpha}$ and the energy eigenvalues $E^{INZ(\pm)}_{\alpha}$ are obtained employing the Hill–Wheeler relation

$$\sum_{K'} \mathcal{H}^{INZ(\pm)}_{K,K'} \; g^{INZ(\pm)}_{K',\alpha} = E^{INZ(\pm)}_{\alpha} \sum_{K'} \mathcal{N}^{INZ(\pm)}_{K,K'} \; g^{INZ(\pm)}_{K',\alpha} \,, \tag{5}$$

with the kernels defined as follows:

$$\left\{ \begin{array}{c} \mathcal{H}^{INZ(\pm)}_{K,K'} \\ \mathcal{N}^{INZ(\pm)}_{K,K'} \end{array} \right\} = \langle \Phi | \left\{ \begin{array}{c} \hat{H} \\ 1 \end{array} \right\} \hat{P}^I_{KK'} \hat{P}^N \hat{P}^Z \hat{P}_{\pm} | \Phi \rangle \,. \tag{6}$$

Interested reader is referred to Ref. [6] for mathematical details, whereas applications to examining the rotational properties of the nuclei in tetrahedral symmetry states can be found in Refs. [6, 8], see also Refs. [2] and [9].

2.2. Quantum rotors with tetrahedral symmetry

Before discussing the consequences of the tetrahedral symmetry on the structure of rotational bands resulting from the application of the angular-momentum projection in the framework of the Gogny mean-field Hamiltonian, it will be instructive to recall the spectral properties of a structureless quantum rotor with tetrahedral symmetry. This problem has been presented in Ref. [10] with the help of the spherical-tensor operator-basis in the form of

$$\hat{T}^{\lambda}_{\mu}(n) = \Bigg(\underbrace{\Big(\Big(\hat{I} \otimes \hat{I} \Big)^2 \otimes \ldots \otimes \hat{I} \Big)^{\lambda-1} \otimes \hat{I}}_{n \text{ times}} \Bigg)^{\lambda}_{\mu} , \tag{7}$$

where $\hat{I} = \{\hat{I}_{-1}, \hat{I}_0, \hat{I}_{+1}\}$ are the collective angular momentum operators and "$\otimes$" refers to the Clebsch–Gordan coupling. Employing Eq. (7), the so-called generalised quantum rotor Hamiltonian (*cf.* Ref. [10] and references therein) can be constructed

$$\hat{H}_{\text{rotor}} = \sum_{n=0}^{\infty} \sum_{\lambda} \left\{ h_{\lambda 0} \hat{T}^{\lambda}_{0}(n) + \sum_{\mu=1}^{\lambda} \left[h_{\lambda\mu} \hat{T}^{\lambda}_{\mu}(n) + (-1)^{\mu} h^{\star}_{\lambda-\mu} \hat{T}^{\lambda}_{-\mu}(n) \right] \right\} , \tag{8}$$

where $h_{\lambda\mu}$ are adjustable constants. This expression reduces to the lowest order tetrahedral symmetry rotor by adjusting the indices λ and μ as follows:

$$\hat{H}^{\text{T}^{\text{D}}}_{\text{rotor}} = \underbrace{h_{00}\, T^0_0(2)}_{\hat{H}_{\text{sph}}(2)} + \underbrace{h_{32}\, \left[T^3_{+2} - T^3_{-2} \right]}_{\hat{H}_{\text{T}_\text{d}}} = \hat{H}_{\text{sph}}(2) + \hat{H}_{\text{T}_\text{d}} \,. \tag{9}$$

Here, $\hat{H}_{\text{sph}}(2) \propto \hat{I}^2$ is by definition a spherically-symmetric second order operator and $\hat{H}_{\text{T}_\text{d}}(3)$ is a third order tetrahedral symmetry operator constructed out of components of $\hat{I}$. The parameters h_{00} and h_{32} can be adjusted to simulate the desired rotational properties of the corresponding spectra. The spectra of the rotor Hamiltonians with tetrahedral symmetry are composed of what we refer to as tetrahedral bands which will be discussed next.

3. Group-theory-induced structure of tetrahedral bands: Implied users instructions for experimental search

In contrast to properties of the rotational bands produced *e.g.* by axially-symmetric nuclei, tetrahedral symmetry bands are composed of states of both parities and in the exact symmetry limit, they contain degenerate multiplets (see below). These properties are unique and allow to identify the corresponding symmetry; the only common feature with the bands known from the literature is the quadratic energy-spin dependence: $E_I \propto I(I+1)$.

3.1. Tetrahedral bands in even–even nuclei: $T_{\rm d}$ group

It can be demonstrated using the exact methods of the point group representation theory that the rotational bands of the tetrahedral symmetry quantum rotors of even–even nuclei like the one in Eq. (9) can be classified according to the 5 irreducible representations of the $T_{\rm d}$ group, here denoted A_1, A_2, E, F_1 and F_2, *cf.* Refs. [7, 8] and references therein. For instance, the bands corresponding to irreducible representation A_1 form a common parabola composed of the following sequence:

$$\mathrm{A}_1 : 0^+,\ 3^-,\ 4^+,\ \underbrace{(6^+, 6^-)}_{\text{doublet}},\ 7^-,\ 8^+,\ \underbrace{(9^+, 9^-)}_{\text{doublet}},\ \underbrace{(10^+, 10^-)}_{\text{doublet}},\ 11^-,\ \underbrace{2\times 12^+,\ 12^-}_{\text{triplet}},\ \dots, \tag{10}$$

whereas the other representations induce the following band structures:

$$\mathrm{A}_2 :\ \ 0^-,\ 3^+,\ 4^-,\ \underbrace{(6^+, 6^-)}_{\text{doublet}},\ 7^+,\ 8^-,\ \underbrace{(9^+, 9^-)}_{\text{doublet}},\ \underbrace{(10^+, 10^-)}_{\text{doublet}},\ 11^+,\ \underbrace{12^+, 2\times 12^-}_{\text{triplet}},\ \dots, \tag{11}$$

$$\mathrm{E} :\ \underbrace{(2^+, 2^-)}_{\text{doublet}}, \underbrace{(4^+, 4^-)}_{\text{doublet}}, \underbrace{(5^+, 5^-)}_{\text{doublet}}, \underbrace{(6^+, 6^-)}_{\text{doublet}}, \underbrace{(7^+, 7^-)}_{\text{doublet}}, \underbrace{(2\times 8^+, 2\times 8^-)}_{\text{quadruplet}}, \underbrace{(9^+,\ 9^-)}_{\text{doublet}}, \dots, \tag{12}$$

$$\mathrm{F}_1 :\ \ 1^+,\ 2^-,\ \underbrace{(3^+, 3^-)}_{\text{doublet}}, \underbrace{(4^+, 4^-)}_{\text{doublet}}, \underbrace{(2\times 5^+,\ 5^-)}_{\text{triplet}}, \underbrace{(6^+, 2\times 6^-)}_{\text{triplet}}, \underbrace{(2\times 7^+, 2\times 7^-)}_{\text{quadruplet}}, \dots, \tag{13}$$

$$\mathrm{F}_2 :\ \ 1^-,\ 2^+,\ \underbrace{(3^+, 3^-)}_{\text{doublet}}, \underbrace{(4^+, 4^-)}_{\text{doublet}}, \underbrace{(5^+,\ 2\times 5^-)}_{\text{triplet}}, \underbrace{(2\times 6^+, 6^-)}_{\text{triplet}}, \underbrace{(2\times 7^+, 2\times 7^-)}_{\text{quadruplet}}, \dots \tag{14}$$

It is worth emphasising that the lowest tetrahedral bands have a unique $I^\pi = 0^+$ ground-state, so that the irreducible representation A_1, *cf.* Eq. (10), plays a distinguished role.

3.2. Tetrahedral bands in odd-A nuclei: $T_{\mathrm{d}}^{\mathrm{D}}$-group

As it is well-known from the group representation theory, the spinor (so-called *double*) point groups differ from the classical point groups both in terms of the numbers of the symmetry elements in the group as well as in terms of numbers and structures of their irreducible representations. The double point group of interest, $\mathrm{T_d^D}$, possesses three irreducible representations introduced already in Sect. 1, denoted E, E* and G.

The first two of them can be recognised as parity-conjugate partners as it can be seen from the following two sequences:

$$\mathrm{E}: \quad \frac{1}{2}^+, \frac{5}{2}^-, \underbrace{\left\{\frac{7}{2}^+, \frac{7}{2}^-\right\}}_{\text{doublet}}, \frac{9}{2}^+, \underbrace{\left\{\frac{11}{2}^+, \frac{11}{2}^-\right\}}_{\text{doublet}}, \underbrace{\left\{\frac{13}{2}^+, 2\times\frac{13}{2}^-\right\}}_{\text{triplet}}, \underbrace{\left\{\frac{15}{2}^+, \frac{15}{2}^-\right\}}_{\text{doublet}}, \ldots, \tag{15}$$

$$\mathrm{E}^*: \quad \frac{1}{2}^-, \frac{5}{2}^+, \underbrace{\left\{\frac{7}{2}^-, \frac{7}{2}^+\right\}}_{\text{doublet}}, \frac{9}{2}^-, \underbrace{\left\{\frac{11}{2}^-, \frac{11}{2}^+\right\}}_{\text{doublet}}, \underbrace{\left\{2\times\frac{13}{2}^+, \frac{13}{2}^-\right\}}_{\text{triplet}}, \underbrace{\left\{\frac{15}{2}^-, \frac{15}{2}^+\right\}}_{\text{doublet}}, \ldots, \tag{16}$$

whereas the third one, G, is composed of parity-multiplets: doublets, quadruplets, sixtuplets, octuplets, *etc.*

$$\begin{aligned}\mathrm{G}: \quad & \underbrace{\left\{\frac{3}{2}^+, \frac{3}{2}^-\right\}}_{\text{doublet}}, \underbrace{\left\{\frac{5}{2}^+, \frac{5}{2}^-\right\}}_{\text{doublet}}, \underbrace{\left\{\frac{7}{2}^+, \frac{7}{2}^-\right\}}_{\text{doublet}}, \underbrace{2\times\left\{\frac{9}{2}^+, \frac{9}{2}^-\right\}}_{\text{quadruplet}}, \underbrace{2\times\left\{\frac{11}{2}^+, \frac{11}{2}^-\right\}}_{\text{quadruplet}}, \\ & \underbrace{2\times\left\{\frac{13}{2}^+, \frac{13}{2}^-\right\}}_{\text{quadruplet}}, \underbrace{3\times\left\{\frac{15}{2}^+, \frac{15}{2}^-\right\}}_{\text{sixtuplet}}, \ldots \underbrace{4\times\left\{\frac{21}{2}^+, \frac{21}{2}^-\right\}}_{\text{octuplet}}, \ldots\end{aligned} \tag{17}$$

As it can be seen from the above relations, again the band structures are unique and characteristic of various combinations of opposite-parity states and multiplets.

3.3. Tetrahedral band identification: User instructions

The rotational band structures presented in Sects. 3.1 and 3.2 define the new branch of nuclear spectroscopy *in statu nascendi*: This is by trying to determine the presence of approximate parabolic structures in these very characteristic forms, which contain doublets, triplets, quadruplets ... of states in the very specific order, that we will be able to determine the presence of the underlying symmetry in subatomic physics. Below, we list in the form of the short phrases which we refer to as 'user instructions' the main strategic lines to follow.

— *Even–even nuclei: Tetrahedral group* T_d. The tetrahedral ground-state band with its $I^\pi = 0^+$ band head is given by the irreducible representation A_1, with the spin-parity sequence defined by Eq. (10). It is characterised by the absence of states with $I = 1$ or 2 and by the presence of parity doublets at $I^\pi = 6^\pm, 9^\pm, 10^\pm$, *etc.* Other tetrahedral symmetry bands, possibly lying higher in the energy scale, have the spin-parity structures given by Eqs. (11)–(14).

— *Even–even nuclei: Octahedral group* O_h. One can profit from the above information in order to conclude about the possible presences of octahedral symmetry. The latter is expected to influence the structure of Eq. (10) in that the states of positive and negative parities form separate parabolic sequences, *cf.* Fig. 5 of Ref. [2] as an example. This double-band structure can be employed as a direct complementary test for the presence of O_h-symmetry.

— *Odd-A nuclei: Tetrahedral double group* T_d^D. The main strategical lines to follow are analogous to the ones just listed: identify the spin-parity sequences predefined by the group theory. However, the group structure of T_d^D is different from the group structure of T_d, and it follows that the detailed structure of the spin-parity sequences for odd-A nuclei differs, as given by Eqs. (15)–(17). A complementary strategy in the research of odd-A nuclei, advocated in Ref. [9], is to combine the first-order Coriolis coupling with the group theory considerations followed in this article. Interested reader is referred to the above article for details.

— *Vanishing dipole and quadrupole moments — mass spectrometry alternative.* An important difficulty established long ago is related to the fact that the tetrahedral and/or octahedral symmetry configurations generate neither collective E1-, nor E2 transitions, the first allowed being E3 — and thus even the most powerful γ-detection systems cannot provide any direct help (see, however, remarks below). Since the usually dominating electro-magnetic signals are expected to be absent, the most natural alternative is to employ the mass-spectrometry techniques and the isomer search, *cf. e.g.* Sect. 3 of Ref. [2].

— *Vanishing dipole and quadrupole moments — population difficulties.* Another difficulty is related to the fact that tetrahedral symmetry states do not generate any electromagnetic transitions of multipolarity lower than $\lambda = 3$ which would enable the detection of their presence; equally importantly they cannot be populated via such transitions. The corresponding 'user instruction' is to find appropriate nuclear re-

actions, which allow for populating the sought states at relatively high excitations energies at not too high (not exceeding the values of the order of a dozen $\hbar$) angular momenta.

— *Particle–hole excited states with tetrahedral deformation-driving orbitals.* At this point, let us emphasise that, in addition to examining the low-lying energy sequences of excited states in even–even and odd-A nuclei in the vicinities of the tetrahedral doubly-magic nuclei with proton and neutron numbers (Z_0, N_0 = 32, 40, 56, 64, 70, 90, 112, 136), one may focus on the specific particle–hole excited configurations in which the hole-level is strongly up-sloping and the particle level is strongly down-sloping. Examples of the corresponding structures are given in Fig. 1. Indeed, consider any one of the two 4-fold degenerate up-sloping orbitals (full lines just below the $N = 82$ gap in Fig. 1, top) and the down-sloping 4-fold degenerate orbital below $N = 94$ gap. The particle–hole excitations involving these orbitals, more precisely $1p$–$1h$ and $2p$–$2h$, are illustrated in Fig. 2.

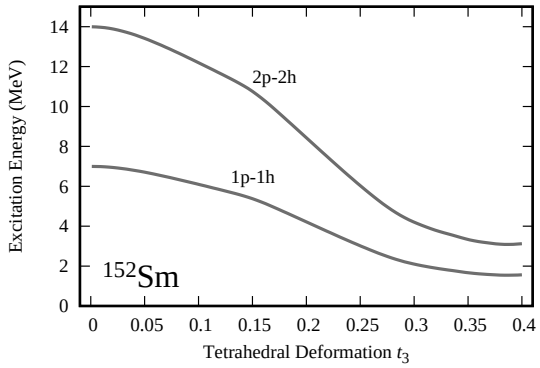

Fig. 2. Excitation energies of selected particle–hole excitations constructed in such a way that the hole orbitals are up-sloping (4-fold degenerate orbital closed to the $N = 82$ gap in Fig. 1, top) and the particle orbitals are down-sloping (4-fold degenerate orbital below $N = 94$ gap, the same figure) as a function of increasing tetrahedral deformation, $t_3 \equiv \alpha_{32}$. Emphasise degeneracy mechanism: the $1p$–$1h$ excitation appears 16-fold degenerate, the $2p$–$2h$ one is 36-fold degenerate.

Let us notice that whereas $1p$–$1h$ excited state gains in energy with tetrahedral deformation increasing more than 5 MeV (within the scale of the figure), the $2p$–$2h$ configuration gains nearly 11 MeV under the same conditions.

Two extra properties deserve noticing.

— *Large tetrahedral deformations far from the magic configurations.* Since the single-particle orbitals change very slowly with the proton and neutron numbers, the behaviour of the two curves selected in this example can be seen as 'universal' in a given mass range. It then follows that it will be sufficient to select the proton and neutron numbers of the discussed nucleus sufficiently far from the magic numbers in such a way that the energy corresponding $0p$–$0h$ configuration is flat in terms of t_3, in which case the excited np–nh states superposed with the $0p$–$0h$ state will likely have a strong t_3-deformation.

— *Extremely high degeneracies of the excited np–nh states.* An important element of consideration are unprecedented degeneracies of the considered states. In the considered example of $2p$–$2h$ configuration, the degeneracy is equal to 36. Without performing any detailed calculations, one may expect that the presence of those high degeneracies should favour (increase the probability of) populating those particular states in the case of tetrahedral (and/or octahedral) deformations.

— *Using γ-multi-detector systems in the search for high-rank symmetries.* From the fact that in the exact symmetry limits, the first non-vanishing electromagnetic radiation is expected to be of the E3-character (thus orders of magnitude weaker than the one of lower multipolarities), one could conclude, perhaps too rapidly, that the γ-detection systems are not very useful. Just on the contrary: One has to remember that most of the predicted tetrahedral-symmetry nuclei are not exactly doubly magic and, moreover, the symmetries are partially (even if weakly) broken by the Coriolis alignment effects on top of which one has to account for the quadrupole zero-point oscillations. All these mechanisms imply dynamical symmetry breaking effects resulting in weak, possibly both E1 and E2 electromagnetic radiation, and the importance of the powerful γ-multi-detector systems should not be under-estimated.

4. Summary and conclusions

In this article, we briefly summarise the recent evolution of the ideas about the identification of the tetrahedral and octahedral symmetries in atomic nuclei. The central arguments are based on the application of the microscopic mean-field theory in the realisation of the spin-parity and particle number projected Hartree–Fock–Bogolyubov approach with the Gogny interactions together with the group-theory results. We provide a compact formulation of the suggestions about the experimental choices in the form of the 'user instructions' which are expected to help optimising the future experiments.

This work was partially supported by the National Science Centre, Poland (NCN) under contract No. 2016/21/B/ST2/01227, the Polish–French COPIN-IN2P3 collaboration agreement under project numbers 04-113 and 05-119 and by the Polish–French collaboration project LEA-COPIGAL.

REFERENCES

[1] X. Li, J. Dudek, *Phys. Rev. C* **49**, 1246 (1994).

[2] J. Dudek *et al.*, *Phys. Rev. C* **97**, 021302 (2018).

[3] J. Dudek, A. Góźdź, N. Schunck, M. Miśkiewicz, *Phys. Rev. Lett.* **88**, 252502 (2002).

[4] The *Universal Woods–Saxon Hamiltonian* and associated, so-called 'universal parametrization' has been developed in a series of articles:
J. Dudek, T. Werner, *J. Phys. G: Nucl. Phys.* **4**, 1543 (1978);
J. Dudek *et al.*, *J. Phys. G: Nucl. Phys.* **5**, 1359 (1979);
J. Dudek, W. Nazarewicz, T. Werner, *Nucl. Phys. A* **341**, 253 (1980);
J. Dudek, Z. Szymański, T. Werner, *Phys. Rev. C* **23**, 920 (1981)
and has been summarized in: S. Ćwiok *et al.*, *Comput. Phys. Commun.* **46**, 379 (1987). This approach is being used without modifications by many authors also today.

[5] J. Dudek *et al.*, *Phys. Rev. Lett.* **97**, 072501 (2006).

[6] S. Tagami, Y.R. Shimizu, J. Dudek, *Prog. Theor. Phys. Suppl.* **196**, 334 (2012).

[7] S. Tagami, Y.R. Shimizu, J. Dudek, *Phys. Rev. C* **87**, 054306 (2013).

[8] S. Tagami, Y.R. Shimizu, J. Dudek, *J. Phys. G: Nucl. Part. Phys.* **42**, 015106 (2015).

[9] S. Tagami, Y.R. Shimizu, J. Dudek, *Phys. Rev. C* **98**, 024304 (2018).

[10] A. Góźdź, M. Miśkiewicz, J. Dudek, *Int. J. Mod. Phys. E* **17**, 272 (2008).